JOURNAL OF MATERIALS SCIENCE 11 (1976) 604–611

# Chemical vapour-deposited silicon nitride

## Part 2 *Density and formation mechanism*

KOICHI NIIHARA, TOSHIO HIRAI
*The Research Institute for Iron, Steel and Other Metals, Tohoku University, Sendai, 980, Japan*

Chemical vapour-deposited $Si_3N_4$ (pyrolytic $Si_3N_4$) has been prepared from a $SiCl_4$ + $NH_3/H_2$ system at 1100 to 1500° C under total pressures of 5 to 300 Torr. The densities of crystalline deposits are 3.15 to 3.18 g cm$^{-3}$, nearly independent of the deposition conditions. On the other hand, the densities of amorphous deposits depend strongly on the deposition conditions and have a minimum value of 2.60 g cm$^{-3}$ at 1200° C and 40 Torr. The deposition rate of Py–$Si_3N_4$ obeys a linear law. The rate of increase in thickness is markedly affected by the deposition conditions, its maximum value being 0.73 mm h$^{-1}$ for cystalline deposits at 1400° C and 40 Torr, and 0.36 mm h$^{-1}$ for the amorphous deposits at 1300° C and 40 Torr. The activation energies of formation of Py–$Si_3N_4$ are 30 to 33 and 53 kcal mol$^{-1}$ for the amorphous and crystalline deposits, respectively. The formation mechanism is also discussed.

## 1. Introduction

Chemical vapour-deposition (CVD) is playing an increasingly important role in the fabrication of intricate shapes and thin films for optical and protective coatings and solid state devices, and of massive products with a high degree of anisotropy for high temperature use. For all of these applications, the controlled deposition of structures and nonstoichiometry of materials is essential. An investigation of the mechanism of CVD would be useful to produce the desired properties.

Deposition of pyrolytic silicon nitride (Py–$Si_3N_4$) by CVD has been carried out using various silicon compounds such as silane [1–8], silicon tetrafluoride [9], silicon tetrachloride [6–8, 10–12], silicon tetrabromide [13] and silica [14, 15] as the feed source of silicon. In general, $SiH_4$ + $NH_3$ and $SiCl_4$ + $NH_3$ systems were frequently employed for the preparation of thin amorphous Py–$Si_3N_4$ films in the electronic micro-device applications [1–7, 10–12, 16, 17].

For the $SiH_4$ + $NH_3$ system, the formation mechanism of thin films of Py–$Si_3N_4$ at low deposition temperatures (750 to 1150° C) has been relatively well established [10–12]. For the $SiCl_4$ + $NH_3$ system, there is an investigation by Grieco *et al.* on the formation mechanism of thin films [10]. However, little is known about the formation mechanism of massive Py–$Si_3N_4$.

Massive Py–$Si_3N_4$ up to 4.6 mm in thickness was prepared in our laboratory using the $SiCl_4$ + $NH_3/H_2$ system ($H_2$: carrier gas) under various deposition conditions. In Part 1 [18] we described the surface morphology, microstructure, colour, composition and cracking of Py–$Si_3N_4$. In this paper, the effects of the deposition temperature and total pressure on the density and deposition rate are investigated, and the formation mechanism of Py–$Si_3N_4$ under the various conditions is discussed.

## 2. Experimental procedure

### 2.1. Preparation of pyrolytic $Si_3N_4$

Py–$Si_3N_4$ was prepared on a directly heated graphite substrate by CVD. The reactant was a mixture of $NH_3$ and $SiCl_4$ carried with hydrogen gas. The detailed process has been described in Part 1 [18], and the deposition conditions of Py–$Si_3N_4$ are summarized in Table I. Fig. 1 shows the effect of the deposition temperature ($T_{dep}$) and the total pressure ($P_{tot}$) on the formation of amorphous and crystalline deposits [18]. The crystal structure of crystalline deposits prepared in this work was $\alpha$–$Si_3N_4$, and free silicon and other silicon compounds were not identified by X-ray diffraction, as mentioned already [18].



© 1976 Chapman and Hall Ltd. Printed in Great Britain.

TABLE I The deposition conditions of Py–$Si_3N_4$

| | |
|---|---|
| *Constant conditions* | |
| Heating method | Direct heating of graphite substrate |
| Flow rate | $SiCl_4$ = 0.8 (in liq.) $cm^3 min^{-1}$ |
| | $NH_3$ = 60 $cm^3 min^{-1}$ |
| | $H_2$ = 700 $cm^3 min^{-1}$ |
| *Variable conditions* | |
| Deposition temperature | 1100 to 1700° C |
| Deposition time | 0.5 to 12 h |
| Total gas pressure | 5 to 300 Torr |

## 2.2. Density measurement

The specimens, 5 x 5 to 5 x 10 mm in size, were prepared by cutting deposits 0.1 to 4.6 mm in thickness together with the graphite substrate and then removing the graphite substrate in a $3HNO_3$–$7H_2SO_4$ solution. The density of deposits was determined by a displacement technique using toluene.

## 2.3. Thickness measurement

The specimens were cut perpendicular to the substrate surface and then metallographically polished. The thickness of Py–$Si_3N_4$ was determined by averaging the values measured at about twenty points of the specimen by a travelling microscope.

## 2.4. Deposition rate

The relation between deposition and time is written as

$$(\Delta w)^n = kt, \quad (1)$$

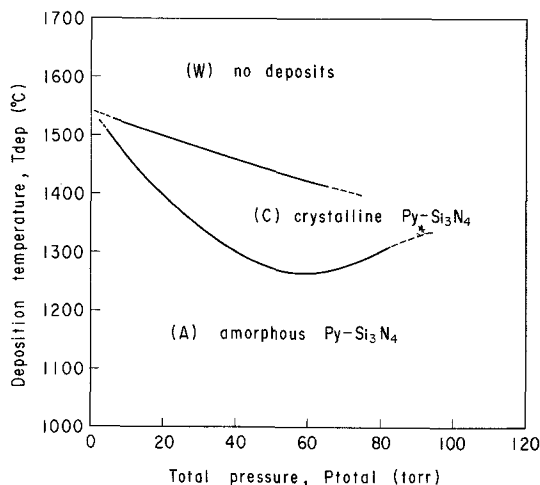


*Figure 1* Effect of deposition temperature ($T_{dep}$) and total pressure ($P_{tot}$) on the crystal structure of Py–$Si_3N_4$ [18].

where $\Delta w$, $n$, $k$, and $t$ are the weight increase of the deposit per unit surface area of the substrate, the order of reaction, the deposition rate constant and the time, respectively. Since $\Delta w$ is equal to the product of density ($D$) and thickness ($x$), we obtain

$$(Dx)^n = kt. \quad (2)$$

The value of $n$ was determined from the time dependence of the deposition.

# 3. Experimental results

## 3.1. Effect of total pressure on density

Fig. 2 shows the relationship between the density ($D$) and $P_{tot}$ at $T_{dep}$ of 1100 to 1400° C. As presented in Fig. 2, $D$ of the amorphous Py–$Si_3N_4$ formed at 1100 and 1200° C decreased with increasing $P_{tot}$ in the range 10 to 40 Torr, increased with $P_{tot}$ in the range 40 to 60 Torr and reached a constant value of about 2.76 g $cm^{-3}$. The lowest and highest values of $D$ were 2.70 g $cm^{-3}$ (85% of the theoretical density of $\alpha$–$Si_3N_4$, $D_{th}$: 3.18 g $cm^{-3}$) and 2.86 g $cm^{-3}$ (90% of $D_{th}$) at

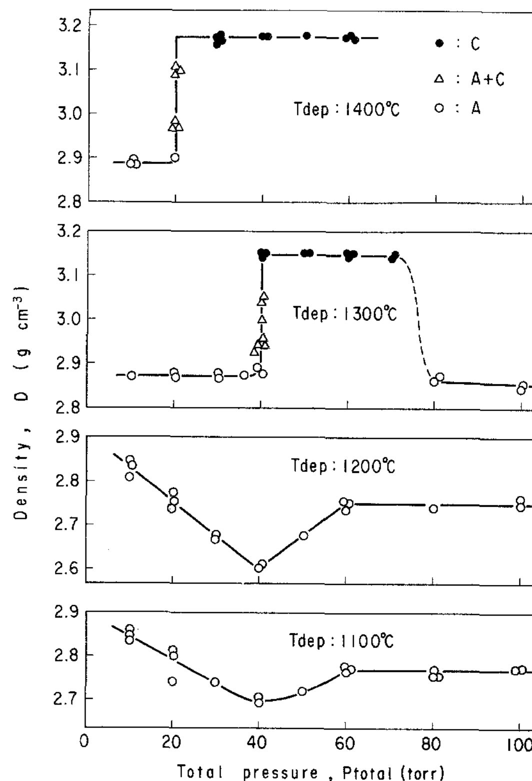


*Figure 2* Effect of total pressure ($P_{tot}$) on density ($D$) obtained at $T_{dep}$ = 1100 to 1400° C. A: amorphous, C: crystalline ($\alpha$–$Si_3N_4$).

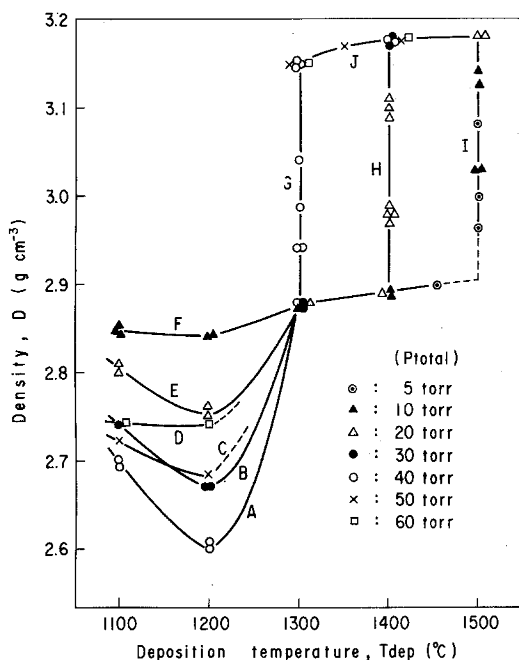


*Figure 3* Effect of deposition temperature ($T_{dep}$) on density ($D$). Curves A, B, C, D, E and F for amorphous deposits, curves G, H and I for mixtures of amorphous and crystalline deposits, and curve J for crystalline deposits.

1100° C, and 2.60 g cm$^{-3}$ (82% of $D_{th}$) and 2.83 g cm$^{-3}$ (89% of $D_{th}$) at 1200° C, respectively. As shown in Fig. 2, $D$ of the deposits prepared at 1300 and 1400° C increased abruptly at 40 and 20 Torr, respectively and decreased at 70 to 80 Torr at 1300° C. These critical $P_{tot}$ values correspond to the pressure at which the amorphous–crystalline transformation occurs. The X-ray diffraction results indicate that the denser deposits are crystalline. At 1300° C, $D$ was 2.88 g cm$^{-3}$ for the amorphous deposits at $P_{tot}$ below 40 Torr and above 80 Torr, and was 3.15 g cm$^{-3}$ for the crystalline deposits between 40 and 80 Torr. The variation in $D$ with $P_{tot}$ at 1400° C was similar to that at 1300° C; $D$ was 2.89 g cm$^{-3}$ for the amorphous deposits at $P_{tot}$ below 20 Torr and 3.18 g cm$^{-3}$ for the crystalline deposits at $P_{tot}$ above 20 Torr. It was likely from Fig. 2 that both $D$ of the amorphous and crystalline deposits at 1300 and 1400° C are independent of $P_{tot}$ in each region.

## 3.2. Effect of deposition temperature on density

The variation in $D$ with $T_{dep}$ is shown in Fig. 3; $D$ was markedly affected by $T_{dep}$. In the case of the amorphous deposits (A to F), the minimum density appeared at 1200° C and 2.60 g cm$^{-3}$ (82% of $D_{th}$). Values of $D$ at the low $P_{tot}$ value (5 or 10 Torr), however, increased gradually with $T_{dep}$ between 1100 and 1450° C. The maximum density for the amorphous deposits was 2.90 g cm$^{-3}$ (91% of $D_{th}$) which was obtained at 1450° C and 5 Torr. Values of $D$ for the crystalline deposits (J) were similar to $D_{th}$ (99 to 100% of $D_{th}$), and increased slightly with the increase of $T_{dep}$. The curves G, H, I, which show the abrupt increase in $D$, correspond to the boundary conditions of 40, 20 and 5 to 10 Torr, respectively (see Fig. 1).

## 3.3. Effect of total pressure on deposition rate

Fig. 4 represents the time dependence of the thickness at 1300° C and 20, 40 and 50 Torr and at 1400° C and 40 Torr. The results at 1300° C and 20 Torr were obtained for the amorphous deposits, those at 1300° C, 50 Torr and at 1400° C, 40 Torr for the crystalline deposits, and those at 1300° C, 40 Torr for mixtures of the amorphous and crystalline deposits. In all cases, it is evident that the formation of Py–$Si_3N_4$ obeys a linear law, that is, $n$ is unity. Therefore, Equation 2 leads to

$$k = Dx/t. \tag{3}$$

Fig. 5 shows the effect of $P_{tot}$ on the rate of increase in thickness ($x/t$) at 1100 to 1500° C. The solid lines indicate the results for amorphous deposits, while the dotted lines for crystalline

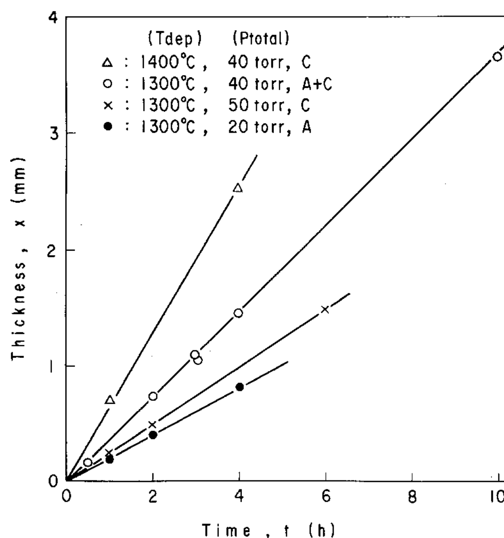


*Figure 4* Time dependence of thickness ($x$).

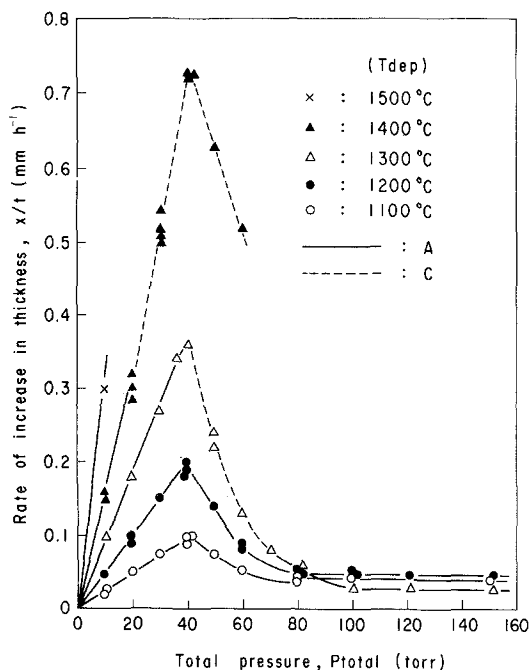


*Figure 5* Effect of total pressure ($P_{tot}$) on the rate of increase in thickness ($x/t$). A: amorphous, C: crystalline ($\alpha$–$Si_3N_4$).

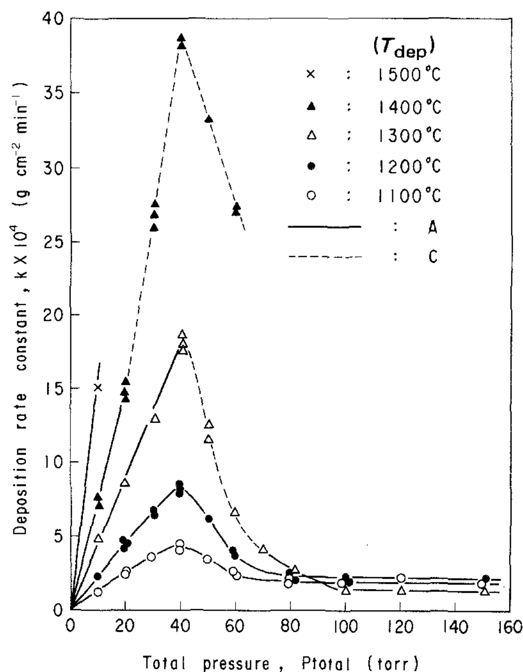


*Figure 6* Effect of total pressure ($P_{tot}$) on deposition rate constant ($k$). A: amorphous, C: crystalline ($\alpha$–$Si_3N_4$).

deposits. As given in Fig. 5, the maximum value of $x/t$ was $0.36\,mm\,h^{-1}$ for the amorphous deposit and $0.73\,mm\,h^{-1}$ for the crystalline deposit prepared at 1300 and 1400° C, respectively, at 40 Torr. The effect of $P_{tot}$ on $x/t$ appears to become stronger with increase in $T_{dep}$. With increasing $P_{tot}$ the values of $x/t$ of amorphous and crystalline deposits increased and decreased at $P_{tot}$ below and above 40 Torr, respectively. Fig. 6 shows the effect of $P_{tot}$ on the deposition rate constant ($k$), which were calculated from the $D$ and $x/t$ data, using Equation 3. As shown in Fig. 6, the appearance of crystalline deposits resulted in a decrease in $k$ and this decrease corresponds to the increase in $P_{tot}$ at 1300° C. At 1400° C, however, $k$ increased with the increase of $P_{tot}$ up to 40 Torr, even after crystalline deposits appeared. At high $P_{tot}$ above 80 Torr, $k$ was small and almost independent of $P_{tot}$.

## 3.4. Effect of deposition temperature on deposition rate

The relations between $k$ and the reciprocal deposition temperature ($1/T_{dep}$) under various deposition conditions are given in Fig. 7. All the datum points lie on straight lines at 10 and 20 Torr, while the plot of $k$ versus $1/T_{dep}$ at 40 and 50 Torr consists of two straight lines. At $P_{tot}$ of 40 and 50 Torr, the gradients below about 1300° C nearly equal those at 10 and 20 Torr. The gradients above 1300° C, however, appeared to be larger than the others. The former was obtained for the crystalline deposits and the latter for the amorphous deposits. This suggests that the formation mechanism of Py–$Si_3N_4$ differs as between the amorphous and

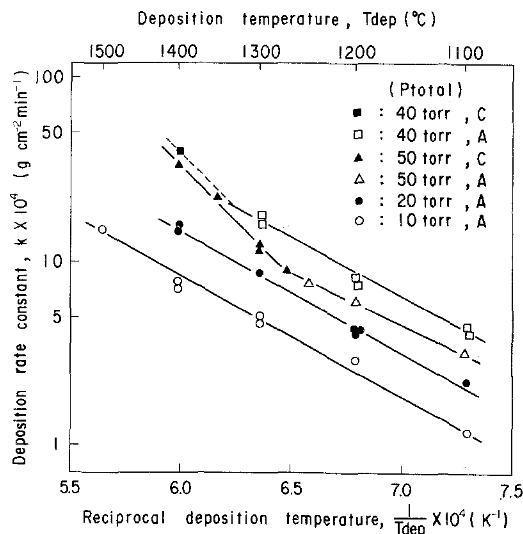


*Figure 7* Arrhenius plot of the deposition rate constant ($k$) under various deposition conditions. A: amorphous, C: crystalline ($\alpha$–$Si_3N_4$).

TABLE II Calculated activation energies of formation of Py–$Si_3N_4$ under various deposition conditions

| Crystal structure* | $P_{tot}$ (Torr) | $T_{dep}$ (° C) | Activation energy, $E$ (kcal $mol^{-1}$) | Reaction type |
|---|---|---|---|---|
| A | 10 | 1100~1500 | 31.6 | 1 |
| A | 20 | 1100~1400 | 30.8 | 1 |
| A | 40 | 1100~1300 | 32.8 | 1 |
| A | 50 | 1100~1250 | 29.6 | 1 |
| C | 50 | 1250~1400 | 53.4 | 2 |

* A: amorphous, C: crystalline (α–$Si_3N_4$).

crystalline deposits. The activation energies ($E$) of formation of Py–$Si_3N_4$ were calculated from Fig. 7 to be 30 to 33 kcal $mol^{-1}$ for the amorphous deposits and about 53 kcal $mol^{-1}$ for the crystalline deposits as listed in Table II.

## 4. Discussion
### 4.1. Density

For amorphous thin films prepared at 950° C, Deal *et al.* [11] and Doo *et al.* [2] reported the $D$ values of 3.2 g $cm^{-3}$ ($x/t$ below 0.0072 mm $h^{-1}$) and 3.02 to 3.21 g $cm^{-3}$ ($x/t$ below 0.003 mm $h^{-1}$), respectively. These values are over $D_{th}$ (3.18 g $cm^{-3}$). Airey *et al.* [8] prepared amorphous coating with $D$ of 2.60 to 2.85 g $cm^{-3}$ ($x/t$ below 0.4 mm $h^{-1}$) at 900 to 1100° C and 2.85 to 3.02 g $cm^{-3}$ ($x/t$ below 0.15 mm $h^{-1}$) at 1150 to 1330° C. Chu *et al.* [6] obtained amorphous thin films at 850 to 1100° C and $x/t$ below 0.002 mm $h^{-1}$. Their results are included in Fig. 8

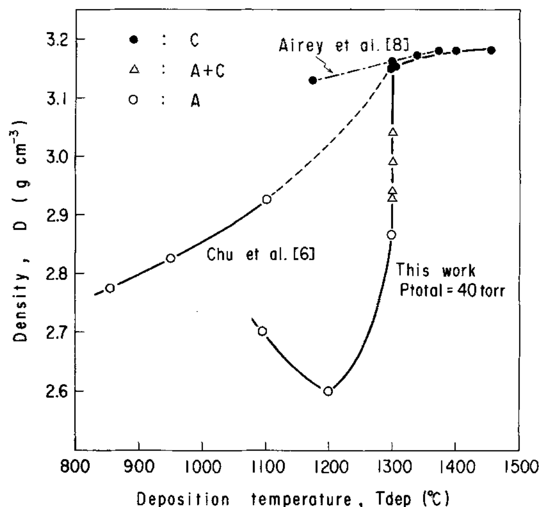


*Figure 9* Relation between deposition temperature ($T_{dep}$) and density ($D$). A: amorphous, C: crystalline (α–$Si_3N_4$).

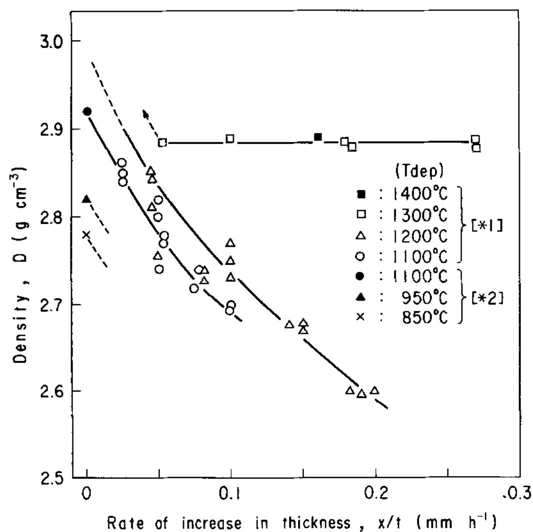


*Figure 8* Relation between the rate of increase in thickness ($x/t$) and density ($D$) for amorphous deposits. A: amorphous, C: crystalline (α–$Si_3N_4$). [*1]: this work, [*2]: Chu *et al.* [6] in the $SiH_4$ + $NH_3$/$NH_3$ system.

which shows the relation between $D$ and $x/t$. At 1100 and 1200° C, $D$ increases with decreasing $x/t$. This indicates that slower $x/t$ forms denser deposits at a constant $T_{dep}$ below 1200° C. At 1300 and 1400° C, $D$ is independent of $x/t$ in this experimental range. At $x/t$ below 0.05 mm $h^{-1}$, however, $D$ may increase abruptly.

The relations between $D$ and $T_{dep}$ as reported by Airey *et al.* [8] and Chu *et al.* [6] for low $x/t$ are shown in Fig. 9 and compared with the present results obtained with high rates of $x/t$. The value of $D$ obtained by extraporating the curve of Chu *et al.* to 1300° C is close to the $D$ values of crystalline deposits (3.15 g $cm^{-3}$). Airey *et al.* [8] prepared the crystalline deposits with 98 to 100% of $D_{th}$ at 1180 to 1380° C and $x/t$ below 0.035 mm $h^{-1}$, which is also shown in Fig. 9. In this work, the crystalline deposits with 99 to 100% of $D_{th}$ were obtained at 1300 to 1500° C and $x/t$ below 0.73 mm $h^{-1}$. The temperature dependence of $D$ for crystalline deposits is in good agreement

with the data of Airey *et al.* [8]. Galasso *et al.* [9] obtained 97 to 100% of $D_{th}$ for the crystalline deposits at 1100 to 1550° C and $x/t = 0.002\,54$ to $0.025\,4\ \mathrm{mm\,h^{-1}}$.

The values of $D$ described above were obtained in various kinds of reactant systems. No remarkable changes in the results were found. For crystalline deposits, $D$ is almost independent of $x/t$, while for amorphous deposits, $D$ is strongly affected by $x/t$.

As reported in Part 1 [18], the several types of microstructures of the surface and the cross-section were observed in deposits prepared under various deposition conditions. For crystalline deposits, $D$ is independent of the microstructure. For amorphous deposits, however, $D$ is closely related to the microstructure, that is, the microstructure of a deposit with the lowest $D$ of $2.60\ \mathrm{g\,cm^{-3}}$ was composed of primary and secondary cones and that with $D$ of $2.85\ \mathrm{g\,cm^{-3}}$ was composed of primary cones. This behaviour is quite similar to that observed in pyrolytic graphite [19]. Observations of the cross-sectional surface of amorphous deposits with cone structures revealed that $D$ decreased with increasing number of cone boundaries. At cone boundaries the amorphous crystallites are aligned in a disordered state, whereupon the intercrystallite porosity increases and consequently $D$ decreases. For the crystalline deposits, most of the crystals have a preferred orientation and there is no mismatch among crystals; the value of $D$ is high.

## 4.2. Deposition rate

Swann *et al.* [20] reported that the rate of increase in thickness of amorphous thin films obeyed a linear law in the case of decomposition of a $SiH_4 + NH_3$ system by a radio frequency glow discharge at $T_{dep} = 300°$ C and $P_{tot} = 10^{-1}$ Torr. For massive deposits, unfortunately, the time dependence of the thickness seems to be unknown. As shown in Fig. 4, the present experiments clarified that the deposition rates of both amorphous and crystalline Py–$Si_3N_4$ obeyed a linear law (Equation 3).

One of the purpose of this experiment is to prepare Py–$Si_3N_4$ at high deposition rates. Table III lists the data of relatively high $x/t$ reported by other workers. Many works have been carried out at low rates of $x/t$ (a few microns per hour), which are not included in Table III.

Grieco *et al.* [10] reported that $x/t$ increased linearly with the partial pressure of $SiCl_4$ between 0.07 and 2 Torr at a constant $NH_3$ partial pressure, and that $x/t$ was independent of $NH_3$ concentration from 4 to 70 Torr at a constant $SiCl_4$ partial pressure. Kohler [7] reported that $x/t$ increased with increase in $SiCl_4$ flow rate, but was independent of $NH_3$ flow rate in the range of 50 to $150\ \mathrm{cm^3\,min^{-1}}$. From these results, it is reasonable that $x/t$ increases linearly with $P_{tot}$ up to 40 Tor (Fig. 5).

On the other hand, $SiCl_4$ reacts with $NH_3$ even at room temperature [10, 21–23].

$$SiCl_4 + 6NH_3 \rightarrow Si(NH)_2 + 4NH_4Cl. \qquad (4)$$

$Si(NH)_2$ polymerizes readily with increasing temperature, and its pyrolysis yields $\alpha$–$Si_3N_4$ according to the following equation:

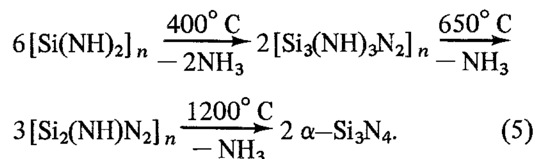

$$6[Si(NH)_2]_n \xrightarrow[-2NH_3]{400°\,C} 2[Si_3(NH)_3N_2]_n \xrightarrow[-NH_3]{650°\,C}$$

$$3[Si_2(NH)N_2]_n \xrightarrow[-NH_3]{1200°\,C} 2\ \alpha\text{–}Si_3N_4. \qquad (5)$$

As seen in Equations 4 and 5, various intermediates contribute to form $Si_3N_4$. In the case of high concentrations of the reactants, these intermediates nucleate and grow in the gas phase to form fine powders $Si_3N_4$ before the deposition of Py–$Si_3N_4$

TABLE III Experimental data on relatively high deposition rates of Py–$Si_3N_4$

| Reactants/carrier | $T_{dep}$ (° C) | $P_{tot}$ (Torr) | Crystal structure* | Deposition rate ($\mathrm{mm\,h^{-1}}$) | Reference |
|---|---|---|---|---|---|
| $SiCl_4 + NH_3/H_2$ | 1000~1200 | 760 | A | 0.06 | 6 |
| $SiH_4 + NH_3/N_2(H_2)$ | 800~1200 | 760 | A | 0.4 | 8 |
| $SiH_4 + NH_3/H_2$ | 600~1200 | 760 | A + C | 0.018 | 1 |
| $SiF_4 + NH_3$ | 1100~1550 | 1~10 | C | 0.0254 | 9 |
| $SiCl_4 + NH_3/N_2$ (Ar) | 1150~1330 | 760 | A | 0.15 | 8 |
| $SiCl_4 + NH_3/N_2$ (Ar) | 1180~1380 | 760 | C | 0.035 | 8 |
| $SiCl_4 + NH_3/H_2$ | 1100~1500 | 5~300 | A | 0.36 | this work |
| $SiCl_4 + NH_3/H_2$ | 1300~1500 | 10~70 | C | 0.73 | this work |

* A: amorphous, C: crystalline ($\alpha$–$Si_3N_4$).

onto the substrate. Consequently, the deposition rate is lowered at higher $P_{tot}$. These two processes overlap and may result in the maximum deposition rate at 40 Torr as shown in Fig. 5. Intermediates have different structures according to decomposition temperature, which may be related to the formation of amorphous and crystalline deposits [24].

Airey *et al.* [8] found that crystalline coatings were obtained at below $x/t = 0.005\,mm\,h^{-1}$ and $0.035\,mm\,h^{-1}$ at 1180 and 1330° C, respectively, and that amorphous coatings were produced above these values at each temperature. Their results indicate that crystal structures depend on the deposition rate. They also reported that crystalline coatings were formed by crystallization and densification of amorphous coatings on the substrate after deposition. However, the time dependence of the density was not observed in the present experiments.

For the $SiH_4 + NH_3/H_2$ and $SiH_4 + N_2H_4/H_2$ systems, $x/t$ reached saturated values at 750 to 1000° C or showed the maximum $x/t$ at about 1000° C in relation between $x/t$ and $1/T_{dep}$ [1, 2, 4, 6]. Doo *et al.* [2] considered that the decrease of $x/t$ at above 1000° C was probably caused by a decrease of the $SiH_4$ concentration near the substrate due to a premature decomposition of $SiH_4$. Furthermore, Sladek [25] discussed theoretically the decrease of $x/t$ as being due to the transition of a completely heterogeneous to a partly homogeneous gas reactions causing cluster formation in the gas phase. In the present experiments (the $SiCl_4 + NH_3/H_2$ system), however, the decrease of $x/t$ was not observed in the range of 1100 to 1500° C below 60 Torr (Fig. 5 and cf. Fig. 7).

The apparent activation energies ($E$) found by other workers for the formation of amorphous Py–$Si_3N_4$ thin films are listed in Table IV. Yoshika *et al.* [4] reported that $E$ ($54\,kcal\,mol^{-1}$) of the amorphous Py–$Si_3N_4$ formation in a $SiH_4 + N_2H_4/H_2$ system at 550 to 650° C was close to the dissociation energy of N–N bond of $N_2H_4$. Consequently, they considered that the N–N bond rupture of $N_2H_4$ is the rate-determining step for the film formation. Other workers have given no interpretation to meanings of the values of the activation energy obtained.

In this work, $E$ for Py–$Si_3N_4$ formation is divided into two varieties; 30 to $33\,kcal\,mol^{-1}$ for amorphous deposits (reaction 1) and ~ 50 $kcal\,mol^{-1}$ for crystalline deposits (reaction 2), as shown in Table II. The formation of Py–$Si_3N_4$ includes complex processes such as decomposition and reaction of reactants, polymerization of products and growth of nuclei in the gas phase or on the deposition surface. Unfortunately, there are almost no thermochemical data concerning various complex intermediates in the $SiCl_4 + NH_3$ system. Therefore, it is difficult to define the meaning of $E$ and subsequently the formation mechanism of massive Py–$Si_3N_4$. The present results imply that the formation mechanism of crystalline deposits differs from that of amorphous deposits.

TABLE IV Literature data on activation energies of formation of amorphous Py–$Si_3N_4$ ($P_{tot}$ = 760 Torr)

| Reactants/carrier | $T_{dep}$ (° C) | $E$ (kcal mol$^{-1}$) | Reference |
|---|---|---|---|
| $SiH_4 + NH_3/H_2$ | 750~1000 | 26.5 | 2 |
| $SiH_4 + NH_3/H_2$ | 1000~1100 | negative | 2 |
| $SiH_4 + NH_3/NH_3$ | 800~950 | 17 | 6 |
| $SiH_4 + NH_3/NH_3$ | 950~1200 | * | 6 |
| $SiH_4 + NH_3/H_2$ | 700~900 | 52 | 1 |
| $SiH_4 + NH_3/H_2$ | 900~1150 | 6 | 1 |
| $SiH_4 + N_2H_4/H_2$ | 550~650 | 54 | 4 |
| $SiH_4 + N_2H_4/H_2$ | 650~1150 | * | 4 |
| $SiCl_4 + NH_3/H_2$ | 850~1225 | 15 | 10 |

* No values are given because $x/t$ is almost independent of $T_{dep}$.

## 5. Conclusions

(1) For amorphous deposits, $D$ has the minimum value at 40 Torr; $2.70\,g\,cm^{-3}$ at 1100° C and $2.60\,g\,cm^{-3}$ at 1200° C. The $D$ value of crystalline deposits is 3.15 to $3.18\,g\,cm^{-3}$, independent of $P_{tot}$.

(2) The relation between $T_{dep}$ and $D$ for amorphous deposits shows the minimum value at 1200° C, which is remarkable at 40 Torr. For crystalline deposits $D$ increases slightly with $T_{dep}$ in the range of 1300 to 1500° C.

(3) The deposition rate of Py–$Si_3N_4$ obeys a linear law.

(4) The effect of $P_{tot}$ on $x/t$ is marked at high $T_{dep}$. At 40 Torr $x/t$ has a maximum value, for example $0.73\,mm\,h^{-1}$ at 1400° C and $0.1\,mm\,h^{-1}$ at 1100° C.

(5) The Arrhenius plots of $k$ indicates straight lines at 10 and 20 Torr and broken lines at 40 and 50 Torr. The activation energies of Py–$Si_3N_4$ formation are 30 to 33 and $53\,kcal\,mol^{-1}$ for the amorphous and crystalline deposits, respectively.

## References


1. K. E. BEAN, P. S. GLEIN, R. L. YEAKLY and W. R. RUNYAN, *J. Electrochem. Soc.* **114** (1967) 733.
2. V. Y. DOO, D. R. NICHOLS and G. A. SILVEY, *ibid* **113** (1966) 1279.
3. V. Y. DOO, D. R. KERR and D. R. NICHOLS, *ibid* **115** (1968) 61.
4. S. YOSHIKA and S. TAKAYANAGI, *ibid* **114** (1967) 962.
5. S. M. HU, *ibid* **113** (1966) 693.
6. T. L. CHU, C. H. LEE and G. A. GRUBER, *ibid* **114** (1967) 717.
7. W. A. KOHLER, *Met. Trans.* **1** (1970) 735.
8. A. C. AIREY, S. CLARKE and P. POPPER, *Proc. Brit. Ceram. Soc.* **22** (1973) 305.
9. F. GALASSO, U. KUNTZ and W. J. CROFT, *J. Amer. Ceram. Soc.* **55** (1972) 431.
10. M. J. GRIECO, F. L. WORTHING and B. SCHWARTZ, *J. Electrochem. Soc.* **115** (1968) 525.
11. B. E. DEAL, E. L. MACHENNA and P. L. CASTRO, *ibid* **116** (1969) 997.
12. H. SEKI and K. MORIYAMA, *Jap. J. Appl. Phys.* **6** (1967) 1345.
13. L. A. ABOAF, *J. Electrochem. Soc.* **116** (1969) 1736.
14. W. F. KNIPPENBERG and G. VERSPUI, Proceedings of the 2nd International Conference on Silicon Carbide (1968) p. 33.
15. K. KIJIMA, N. SETAKA, M. ISHII and H. TANAKA, *J. Amer. Ceram. Soc.* **56** (1973) 346.
16. C. R. BARNES and C. R. GEESNER, *J. Electrochem. Soc.* **107** (1960) 98.
17. P. S. SCHAFFER and B. SWAROOP, *Ceram. Bull.* **49** (1970) 536.
18. K. NIIHARA and T. HIRAI, *J. Mater. Sci.* **11** (1976) 593.
19. S. YAJIMA, T. SATOW and T. HIRAI, *J. Nuclear Mat.* **17** (1965) 127.
20. R. C. G. SWANN, R. R. MEHTA and T. P. CAUGE, *J. Electrochem. Soc.* **114** (1967) 713.
21. M. BILLY, *Ann. Chem.* **4** (1959) 795.
22. O. GLEMSER and P. NAUMANN, *Z. Anorg. Allgem. Chem.* **298** (1958) 134.
23. K. S. MAZDIYASNI and C. M. COOKE, *J. Amer. Ceram. Soc.* **56** (1973) 628.
24. A. KATO, Y. ONO, S. KAWAZOE and I. MOCHIDA, *Yogyo-Kyokai-Shi* **80** (1972) 28.
25. K. J. SLADEK, *J. Electrochem. Soc.* **118** (1971) 654.


Received 3 September and accepted 9 September 1975.